RSC Sustainability

ROYAL SOCIETY OF CHEMISTRY

PAPER

View Article Online
View Journal | View Issue

Cite this: *RSC Sustainability*, 2024, **2**, 3500

Promoting uniform zinc coatings through the use of quaternary ammonium salts based on phthalimide as electroplating additives†

Kexin Du, Xuyang Li, Wenhao Zhou, Peikun Zou, Nayun Zhou, Xin Chen and Limin Wang *

Received 2nd July 2024
Accepted 30th September 2024

DOI: 10.1039/d4su00343h

rsc.li/rscsus

Five quaternary ammonium salts derived from phthalimide compounds (**PI1** to **PI5**) were synthesized and used for the first time as additives in zinc electroplating. Electrochemical experiments and theoretical calculations identified **PI4** as the most effective compound for inhibiting zinc deposition and enhancing electrode adsorption among these compounds. Scanning Electron Microscopy (SEM), Atomic Force Microscopy (AFM), and X-ray Diffraction (XRD) confirmed that **PI4** significantly improves the uniformity and compactness of the zinc coatings. Moreover, the role of **PI4** in zinc electroplating was elucidated. It reduces the interfacial tension between the electroplating solution and the substrate surface, facilitating uniform deposition of metal ions on the substrate, thus resulting in smoother and more adherent coatings. This study provides insights for future research on aqueous zinc-ion batteries, particularly regarding zinc anodes, and also provides a way for sustainable development.

Sustainability spotlight

Conventional electroplating processes involve heavy metals and hazardous chemicals, which can cause serious contamination of water and soil if not handled properly. Therefore, the development of low-toxicity or non-toxic zinc plating additives is the key to achieving sustainable plating. We investigated a quaternary ammonium salt derivative based on phthalimide as a parent, as an electroplating zinc additive, which can achieve uniform deposition of plating layer in the electroplating process. It effectively promotes the development of the zinc electroplating industry in a more environmentally friendly and sustainable direction. Our work emphasizes the importance of the following UN Sustainable Development Goals: affordable and clean energy (SDG 7), industry, innovation and infrastructure (SDG 9).

Introduction

In comparison to lithium-ion batteries, which are characterized by high costs and safety concerns, aqueous zinc-ion batteries (AZBs) garner considerable attention due to their affordability, eco-friendliness, resource abundance, significant theoretical specific capacity (820 mA h g^{-1}), reduced overpotential (−0.76 V *vs.* standard hydrogen electrode), and enhanced volumetric energy density (approximately triple that of lithium metal).[1–4] Consequently, AZBs are poised to supplant lithium-ion batteries in extensive energy storage applications, heralding a new era of sustainable energy storage solutions.[5,6] However, the utility of zinc anodes is compromised by the uneven dissolution and deposition of zinc metal, which can lead to dendrite formation, anode perforation, and detachment of electrode ears, culminating in battery failure and inhibiting deep discharge.[7–9] The development of zinc dendrites severely affects the battery's life cycle. Similar to conventional electroplating processes, irregular electric fields, and zinc ion distribution during zinc electroplating and dissolution contribute to non-uniform zinc deposition, prompting dendrite formation.[10–13] By adopting proven electroplating techniques, uniform zinc coatings can be achieved. Electroplating additives, widely applied in traditional processes, have been successfully used in zinc secondary batteries to inhibit dendritic growth, where adding a trace amount to the electrolyte can considerably enhance the zinc anode's surface smoothness and compactness, multiplying the anode's life cycle manifold.

The evolution of zinc metal plating spans nearly two centuries, with the electroplating process frequently necessitating specific additives to enhance plating solution performance and coating quality.[10] For instance, the application of Metal–Organic Frameworks (MOFs) as protective interfacial layers has demonstrated effectiveness in suppressing dendrite formation, enhancing zinc ion transport, and promoting uniform zinc deposition. Additionally, Covalent Organic Frameworks (COFs),

Shanghai Key Laboratory for Functional Materials Chemistry and Institute of Fine Chemicals, School of Chemistry and Molecular Engineering, East China University of Science and Technology, 130 Meilong Road, Shanghai 200237, P. R. China. E-mail: wanglimin@ecust.edu.cn

† Electronic supplementary information (ESI) available. See DOI: https://doi.org/10.1039/d4su00343h

another class of materials used in zinc-ion batteries, serve as artificial solid electrolyte interfaces (ASEIs) to guide uniform ion diffusion and mitigate side reactions such as zinc corrosion and hydrogen evolution.[14–18] Furthermore, Deep Eutectic Solvents (DESs) have shown potential as innovative electrolyte alternatives, effectively stabilizing zinc anodes by regulating solvation structures, thereby reducing dendrite growth and enabling reversible zinc deposition.[16,19] Similarly, Ionic Liquids (ILs) have been explored for their high ionic conductivity and ability to suppress dendrite formation, offering stable long-term cycling performance.[20]

Building upon this knowledge, the present study employs phthalimide as a zinc electroplating additive, examining its influence on the grain size and surface morphology of zinc coatings. The synthesis of five phthalimide-based quaternary ammonium salts and subsequent electrochemical analyses revealed their substantial inhibitory effects on zinc deposition. Quantum chemical computations identified the **PI4** compound as possessing optimal electrochemical properties and adsorption capabilities. Employing **PI4** in practical electroplating processes, analyses through Scanning Electron Microscopy (SEM), Atomic Force Microscopy (AFM), and X-ray Diffraction (XRD) confirmed **PI4**'s efficacy in promoting uniform zinc deposition. The exploration of **PI4**'s mechanism of action provides a foundation for future research into its application as an electrolyte additive in aqueous zinc-ion batteries, potentially enhancing their performance and sustainability.

Experimental

Synthesis and characterization of materials

Using commercially available *N*-(4-bromobutyl) phthalimide as the raw material, five water-soluble quaternary ammonium compounds, **PI1**–**PI5**, were synthesized by introducing a pyridyl group. The incorporation of the quaternary ammonium structure not only enhanced the water solubility of phthalimide compounds but also provided positive ion centers for their adsorption on the cathode surface. Consequently, the adsorption capacity of phthalimide compounds on the copper surface was significantly augmented. The molecular structures of the five synthesized quaternary ammonium salts are illustrated in Fig. 1, and the detailed synthesis route is delineated in Scheme 1. All other chemicals were procured from commercial sources.

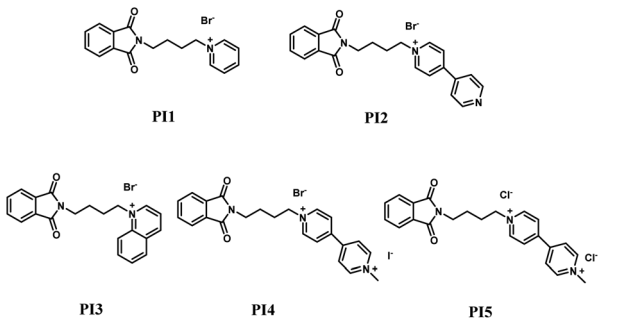

Fig. 1 Molecular structures of quaternary ammonium salts (PI1–PI5).

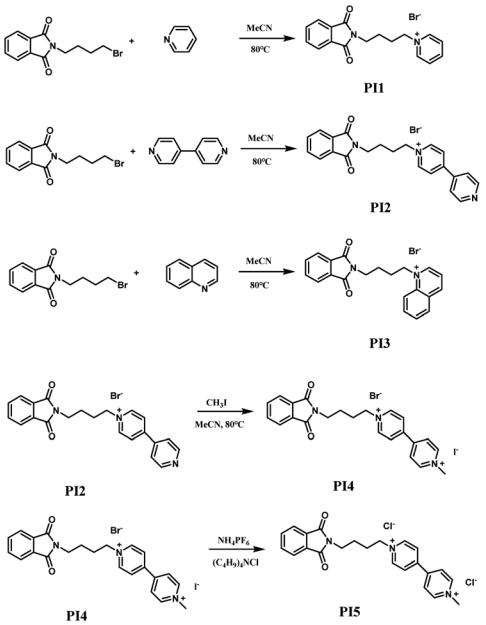

Scheme 1 Synthesis route of quaternary ammonium salts (PI1–PI5).

All the synthesized products were carefully characterized by ^{1}H NMR, ^{13}C NMR (tetramethylsilane as the internal standard, dissolved in DMSO-d_6 at room temperature, and recorded at 400 MHz and 100 MHz, respectively), and high-resolution mass spectrometry (tested and recorded using a Thermo Scientific QE plus using ESI as the ion source) to ensure the accuracy of the structure.

Electrochemical analysis

A series of electrochemical characterization studies of the synthesized additives were conducted through cyclic voltammetry (CV) measurements and kinetic potential polarization. The initial plating solution for all electrochemical tests comprised 1 M $ZnSO_4 \cdot 7H_2O$. The two-electrode system for these tests comprised a 1 cm × 1 cm titanium sheet as the positive electrode and a 1 cm × 1 cm zinc sheet as the negative electrode. Cyclic voltammetry experiments were executed with scanning potentials ranging from 1.0 to −0.2 V at a constant scanning rate of 10 mV s^{-1}. In the kinetic potentiodynamic polarization tests, a constant scanning rate of 10 mV s^{-1} was maintained while the scanning potentials ranged from 0 to −0.2 V.

Computational details

All calculations were conducted utilizing Density Functional Theory (DFT) employing the B3LYP/6-311G method in Gaussian 09 and GaussView 5.0. Structure optimization and frequency calculations ensured that all structures attained true minima in the potential energy plane. Frontier molecular orbital energies, comprising the highest occupied molecular orbital (EHOMO) and the lowest unoccupied molecular orbital (ELUMO), were computed for all compounds to facilitate compound analysis.[21,22] Electrostatic potential (ESP), average local ionization

energy (ALIE), and Fukui function (FF) were visualized using the Multiwfn program.[23–30] Additionally, the planar parameters of the structurally optimized compounds were calculated utilizing the Multiwfn software.[30–33]

Material characterization

A 250 mL hall tank was utilized, containing 1 M $ZnSO_4 \cdot 7H_2O$ as the electrolyte. The negative electrode comprised a zinc plate, while the positive electrode consisted of a copper plate. A current of 1.5 A was applied, and after a discharge period of 30 minutes, the surface morphology and roughness of the deposited zinc coating on the copper sheet were examined using scanning electron microscopy (SEM) with a ZEISS Gemini SEM 300 and atomic force microscopy (AFM). The Bruker Dimension Icon was employed for this purpose. Additionally, the crystal orientation under various conditions was observed using an X-ray diffractometer (Rigaku D/max-2200 PC, Japan).

Results and discussion

Cyclic voltammetry

In the evaluation of electroplating additives through cyclic voltammetry, the diminution of the curve's oxidation reaction area upon the incorporation of additives into the base electroplating solution signifies the inhibition of zinc ion to zinc conversion by the additives. Fig. 2 presents the cyclic voltammetry curves for **PI1** to **PI5** at varying concentrations, where the respective positive and negative peaks denote zinc's deposition and dissolution phases. An observed reduction in curve area with increasing additive concentration suggests a corresponding increase in the difficulty of zinc deposition. This effect is attributed to the competitive adsorption of additives with zinc ions on the cathode surface, thereby impeding zinc deposition. The inhibition efficiency of the five additives is enhanced with concentration, notably with **PI4** exhibiting the most substantial inhibitory effect.

Potentiodynamic polarization measurements

To further ascertain the inhibitory efficacy of quaternary ammonium salts **PI1** to **PI5** on zinc deposition, their dynamic potential polarization curves were examined. The inflection point in these curves, marked by a swift upsurge in current density, signifies the commencement of rapid zinc deposition. This inflection point, the deposition reduction or polarization potential of zinc, correlates positively with the compound's inhibitory strength – the higher the polarization potential, the stronger the inhibition. Fig. 3 illustrates the cathodic polarization curves of the additives at different concentrations, where an increase in zinc's deposition potential post-additive introduction is observable, indicative of additive adsorption on the cathode surface under electrochemical influence, thus elevating cathodic overpotential. The extent of cathodic overpotential enhancement varies among the additives, with **PI4** demonstrating the most pronounced effect, indicative of its superior inhibition of zinc deposition. An increase in additive concentration correlates with a rise in zinc deposition potential, confirming a concentration-dependent inhibitory effect aligned with the cyclic voltammetry findings.

Integrating results from cyclic voltammetry and polarization curve analyses, the inhibitory strengths of the phthalimide quaternary ammonium salts rank as follows: **PI4** > **PI5** > **PI2** >

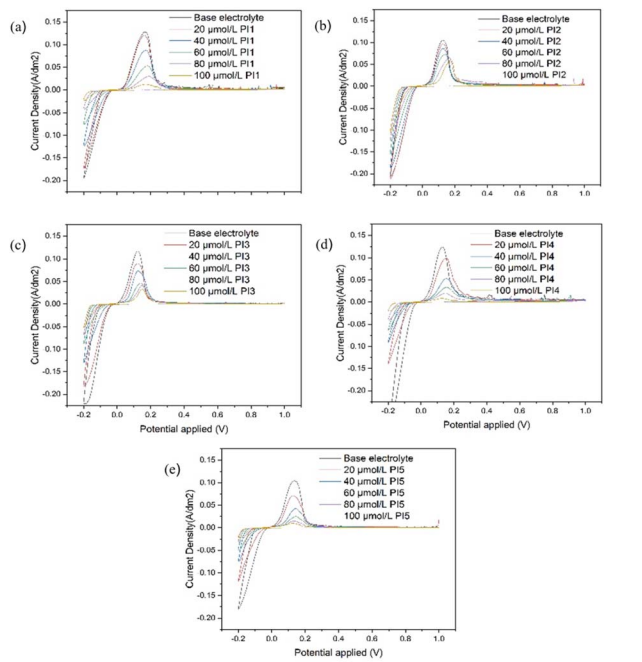

Fig. 2 Cyclic voltammetric curves using different concentrations of PI additives. (a) **PI1**; (b) **PI2**; (c) **PI3**; (d) **PI4**; (e) **PI5**.

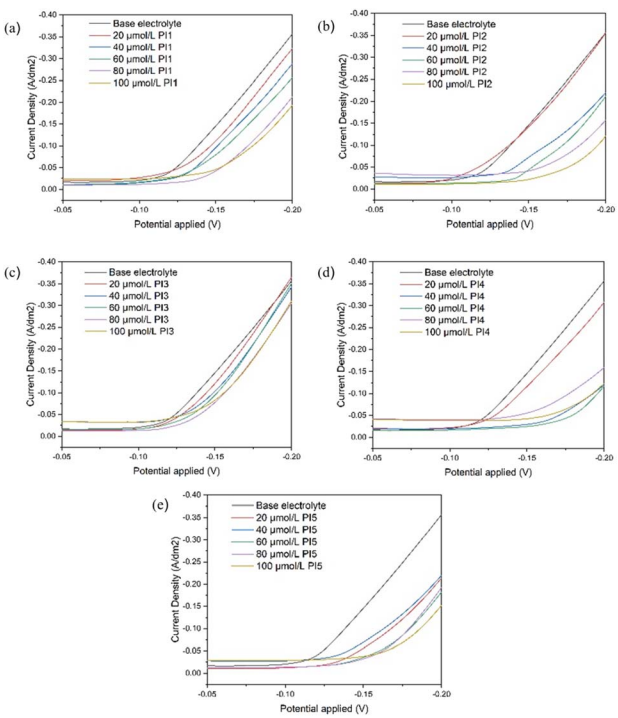

Fig. 3 Polarisation curves using different concentrations of PI additives. (a) **PI1**; (b) **PI2**; (c) **PI3**; (d) **PI4**; (e) **PI5**.

PI1 > **PI3**. The inhibition of the compound can improve the formation of uneven zinc layers due to rapid deposition. A comparative analysis of the molecular structures reveals that **PI2**, which sources its N^+ ions from bipyridine, demonstrates a more potent inhibition than **PI1**, which utilizes pyridine. The comparison between **PI2** and **PI4** suggests that the presence of dual charges amplifies the adsorption efficacy and surface area of the quaternary ammonium salts, facilitating more effective surface adsorption and resultant inhibition. Furthermore, contrasting **PI4** with **PI5** suggests that iodide ions exhibit a stronger inhibitory effect compared to bromide ions, reinforcing the correlation between molecular structure and inhibitory performance. This comprehensive analysis underscores the nuanced interplay between molecular structure and electroplating inhibition, offering valuable insights for the development of more effective electroplating additives.

Energy gap calculations

To prove the inhibition ability of the five synthesized quaternary ammonium phthalimide salts on zinc deposition, the relevant molecular orbitals were calculated using density functional theory, and the structures of the five quaternary ammonium salts **PI1**–**PI5** were optimized. Fig. 4 shows the geometric structure and electron cloud density optimization results of **PI1**–**PI5**. The HOMO of **PI1**–**PI5** is mainly located in the phthalimide region, which means that in the molecular structure of the five phthalimide quaternary ammonium salts, the phthalimide region is more likely to give electrons to metal ions than other regions, thus forming ligands. LUMO is distributed in the pyridine/bipyridine region, which means that the pyridine/bipyridine region is more likely to obtain electrons than other regions, and thus adsorb on the cathode surface. **PI4** and **PI5** have the same parent structure, so they can be regarded as one. Based on electrochemical evaluations, **PI4** demonstrates a more potent inhibitory effect than **PI5**, leading to the exclusion of **PI5** from further consideration. The calculation results are shown in Fig. 4 and Table 1. According to the frontier orbital theory, the highest occupied orbital HOMO shows the ability of the compound to give electrons, the lowest unoccupied orbital LUMO shows the ability of the compound to absorb electrons, and the difference between the two energies ΔE, that is, the energy gap, reflects the stability of the adsorption coating of the molecule on the copper surface to a certain extent, as follows:

$$\Delta E = E_{\mathrm{LUMO}} - E_{\mathrm{HOMO}}$$

The smaller the energy gap of the compound, the greater the adsorption capacity of the metal. According to the energy gap calculation results, it is inferred that the inhibition capacity of the four phthalimide quaternary ammonium salts ranges from large to small as **PI4** > **PI1** > **PI2** ≈ **PI3**, which is slightly different from the electrochemical results (**PI4** > **PI2** > **PI1** > **PI3**). This phenomenon also exists in previous studies, because the electrochemical test was conducted in zinc sulfate solution. However, the simulation calculation is in a vacuum environment, so there are certain differences.[34] Consistent with the electrochemical test results, the quaternary ammonium salt **PI4** has the smallest bandgap ΔE = 0.02185 eV, which is much smaller than the ΔE values of the other four quaternary ammonium salts. This indicates that **PI4** has the strongest adsorption capacity, which explains why the compound **PI4** has the strongest inhibition capacity.

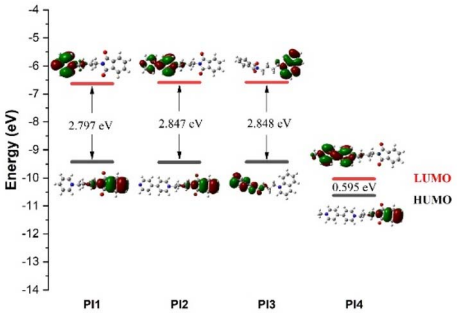

Fig. 4 Distributions and orbital energy values of the highest occupied molecular orbital (HOMO) and the lowest unoccupied molecular orbital (LUMO) of PI additives.

Table 1 Orbital energies (E_{HOMO}, E_{LUMO} and ΔE) of PI additives

Leveler	E_{HOMO} (eV)	E_{LUMO} (eV)	ΔE (eV)
PI1	−9.423	−6.627	2.797
PI2	−9.435	−6.588	2.847
PI3	−9.423	−6.576	2.848
PI4	−10.626	−10.031	0.595

Fukui function calculation

The presented Fig. 5 illustrates the Fukui function calculations for four compounds. In Fig. 5(a) and (b), the maximum positive (f^+) and the most negative (f^-) values of the Fukui function are observed, indicative of the propensity for electron donation and affinity, respectively. Fig. 5(a) demonstrates the highest propensity for electron loss, marked on the green region (1.13 kcal mol^{-1}), while the greatest tendency for electron gain is depicted on the blue region (−0.36 kcal mol^{-1}). In Fig. 5(b),

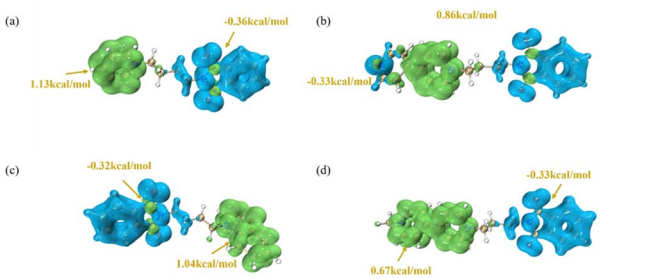

Fig. 5 Fukui function calculation of four PI additives. (a) PI1; (b) PI2; (c) PI3; (d) PI4.

the area most prone to electron loss is similarly indicated in the green region (0.86 kcal mol^{-1}), with the blue region denoting the locus of favored electron gain (−0.83 kcal mol^{-1}). Fig. 5(c) and (d) reveal the Dual Descriptor (DD) of the Fukui function, where yellow arrows point to the maximal positive values, signifying the most favorable positions for electron acquisition, and blue arrows indicate the maximal negative values, suggesting regions more inclined to electron release. Fig. 5(c), the highest positive DD value is 1.04 kcal mol^{-1} and the greatest negative value is −0.32 kcal mol^{-1}. In Fig. 5, the highest positive DD value decreases to 0.67 kcal mol^{-1}, and the greatest negative value is −0.33 kcal mol^{-1}. These calculations provide crucial insights into local variations in electron density, enabling predictions and interpretations of the compounds' reactivity differences in electrochemical reactions.

Calculation of electrostatic potential and average local ionization energy

To further analyze the electron density distribution of the quaternary ammonium salt molecule **PI4**, electrostatic potential energy (ESP) analysis was conducted based on optimal structure optimization to describe the electron density distribution within the molecule. As illustrated in Fig. 6, the red regions denote areas of low electron density, while the blue regions represent areas of high electron density. The intensity of the color signifies the degree of electron density (low/high). The point of maximum electrostatic potential indicates positions with the highest electrostatic adsorption activity under the influence of an electric field. The bipyridine ring portion of the **PI4** molecule exhibits notably high electrostatic potential values, suggesting strong electrostatic adsorption capacity and preference in this region. Consequently, it is more prone to firm adsorption on the copper surface through physical adsorption during deposition.

In addition, the ALIE diagram depicts the distribution of the average ionization energy of the molecule, and the point with the very small value of the average ionization energy is the position with the highest electronic activity. As can be seen from Fig. 7, the very small value points of the average ionization energy of the **PI4** molecule are concentrated on the parent phthalimide,

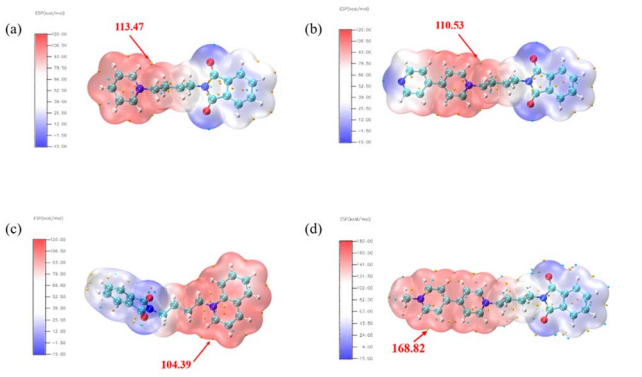

Fig. 6 Electrostatic potential energy (ESP) of the four additives. (a) **PI1**; (b) **PI2**; (c) **PI3**; (d) **PI4**.

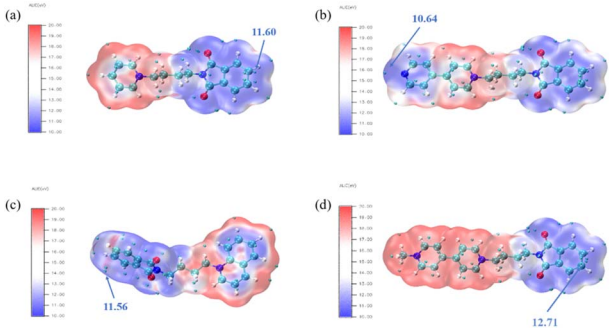

Fig. 7 Average local ionization energy (ALIE) mapped van der Waals surface (*i.e.*, $\rho = 0.001$ a.u. isosurface) of four additives. (a) **PI1**; (b) **PI2**; (c) **PI3**; (d) **PI4**.

showing that it has a high electrophilic reactivity, and is easy to form an adsorption coating by chemisorption through the electrophilic reaction with the copper surface in the deposition. Through quantum chemical calculations, it can be found that **PI4** adsorbs on the copper surface through high physical adsorption (electrostatic adsorption) and high chemical adsorption (electrophilic reaction), which play a leveling role.

Effect of PI4 on the surface morphology of Zn depositing coatings

The electrochemical tests and theoretical calculations described above indicate that **PI4** is the most effective additive. To validate the efficacy of zinc metal anodes in actual electroplating, a discharge simulation was conducted using a Hall bath with both a base bath and a bath containing 100 μmol L^{-1} **PI4** added, each subjected to a current of 1.5 A for half an hour. The surface morphology of the Zn coating was observed using scanning electron microscopy, atomic force microscopy, and X-ray diffraction. As depicted in Fig. 8(a and b), the electroplating coating under the basic electrolyte exhibited large grains, roughness, numerous voids, and significant inconsistency.

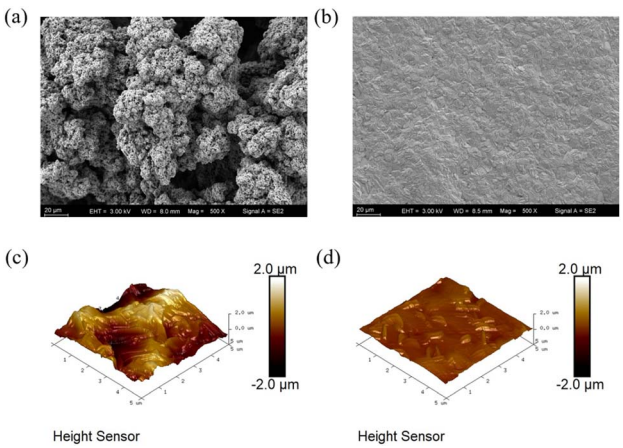

Fig. 8 (a and b) SEM images; (c and d) AFM images were obtained under the conditions of original electrolyte and **PI4** electrolyte respectively at 1.5 A current for 30 min.

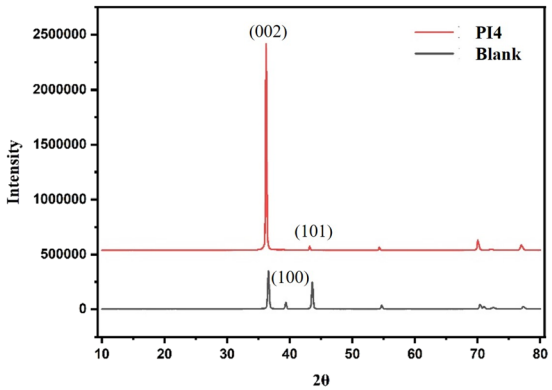

Fig. 9 XRD images were obtained under the conditions of the original electrolyte and PI4 electrolyte respectively at 1.5 A current for 30 min.

Conversely, with the addition of 100 μmol L^{-1} **PI4**, the coating appeared more uniform and finer, forming a cohesive sheet. This indicates that the presence of **PI4** compounds promotes an increase in grain number and a decrease in individual grain size. Fig. 8(c and d) display the results of atomic force microscope scanning. The surface of the coating under the basic electrolyte was covered with numerous tips and voids, resulting in an Ra value of 474 nm. However, the surface roughness of the coating obtained with the additive electrolyte was improved, with the Ra value reduced to 97.8 nm.

Fig. 9 shows the XRD pattern. According to the minimum energy principle, crystals tend to expose more low-energy crystal faces. Theoretically, because Zn(002) has the highest surface symmetry, the highest atomic packing density, and the fewest unsaturated bonds, the surface energy of Zn(002) is the lowest (0.33 J m^{-2}).[35] During electroplating, this structural feature facilitates the epitaxial growth of Zn^{2+} on the edge instead of on the top, which will fundamentally inhibit the growth of dendrites. Therefore, zinc tends to expose the (002) surface during crystallization, which is also the reason why zinc deposition morphology is usually hexagonal thin.[36,37] In addition, the (002) plane can effectively inhibit the HER and corrosion reactions due to its high H adsorption-free energy and Zn atom stripping energy. It can be seen from the figure that the crystal surface orientation is (002) after adding the **PI4** additive, indicating that adding **PI4** can effectively inhibit the HER and corrosion reaction.

Contact angle test

The wettability of the coating surface plays a crucial role in ionic exchange at the interface. The contact angles on the zinc foil with and without additives were measured using a contact angle goniometer, as shown in Fig. 10. The contact angle of the

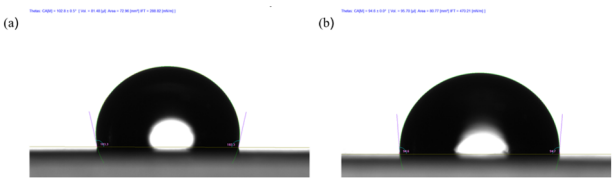

Fig. 10 Contact angle zinc foil (a) without additives; (b) with PI4.

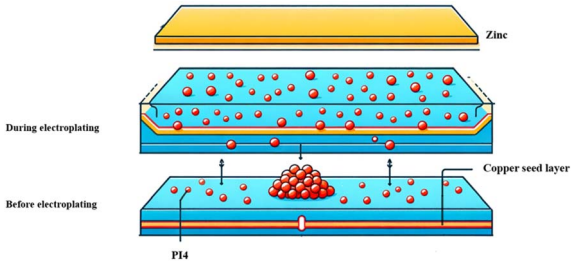

Fig. 11 Mechanism of action of PI4 compound in the electro-galvanizing process.

electrolyte without additives was 103.3°, which decreased to 94.6° after the addition of **PI4**, indicating improved wettability of the interface. Thermodynamically, enhanced interface wettability reduces the free energy of heterogeneous nucleation within cap-shaped droplets, facilitating the uniform distribution of zinc ions on the substrate surface. This promotes a smoother and more even deposition surface.

Mechanistic analysis

The action mechanism of **PI4** in the zinc plating process, as illustrated in Fig. 11, is elucidated based on current experiments and the existing literature. Initially, the dispersion of the additive on the substrate is relatively sparse, likely due to the initial weak interaction between **PI4** and the substrate. As plating advances, electric current, and zinc ion concentration variations lead to the additive's accumulation in specific areas, creating denser adsorption zones. **PI4** molecules, acting as surfactants, are attracted to the substrate surface in the plating solution, forming an adsorption layer that reduces the interfacial tension between the solution and substrate, promoting uniform metal ion deposition.

Conclusions

This study marks the first application of phthalimide-based quaternary ammonium salts (**PI4**) as zinc electroplating additives, thoroughly investigating their mechanisms in the plating process. Electrochemical evaluations reveal that all five synthesized quaternary ammonium salts exhibit varying degrees of inhibition on zinc deposition, with **PI4** standing out due to its significant inhibitory effect. Compared with the commonly used additive benzotriazole (BTA), **PI4** can not only effectively inhibit the formation of dendrites, but also improve the uniformity and densification of the coating. In addition, **PI4** shows a more efficient inhibition effect through its electrochemical properties, while BTA can form a protective film, but the stability of the passivation film during the long-term plating process is not as good as the uniform deposit layer formed by **PI4** additives. Theoretical analysis shows that **PI4** possesses strong physical and chemical adsorption capabilities on the substrate, reducing interfacial tension and promoting uniform metal ion deposition. Compared with additives such as MOFs, COFs, DESs, and ILs, **PI4** can not only effectively promote uniform zinc deposition, but also provide more optimized

surface characteristics, which provide valuable theoretical and experimental basis for further improving the performance of zinc batteries. This comprehensive study offers insights into the potential applications of phthalimide-based materials in aqueous zinc-ion batteries, highlighting the additive's advantages in enhancing battery performance and durability. Further experiments can be conducted to verify the consistency and effectiveness of **PI4** in large-scale electroplating systems. At the same time, the stability and durability of **PI4** during long-term electroplating cycles require further investigation, including evaluation of long-term performance.

Data availability

All data supporting the findings of this study are available within the paper and its ESI.†

Conflicts of interest

There are no conflicts to declare.

Acknowledgements

This research was financially supported by the National Natural Science Foundation of China (21772039 and 21272069) and Sinopec Seeding Program (ZC0607-0869), and we gratefully acknowledge financial support from the Central Universities and Science and Technology Commission of Shanghai Municipality (21DZ2305000). Support from the Fundamental Research Funds for the Central Universities (SLA13223001) is also gratefully acknowledged.

Notes and references

1 M. Song, H. Tan, D. Chao and H. J. Fan, *Adv. Funct. Mater.*, 2018, **28**, 1802564.
2 F. Wan, L. L. Zhang, X. Y. Wang, S. S. Bi, Z. Q. Niu and J. Chen, *Adv. Funct. Mater.*, 2018, **28**, 8.
3 D. L. Han, Z. X. Wang, H. T. Lu, H. Li, C. J. Cui, Z. C. Zhang, R. Sun, C. N. Geng, Q. H. Liang, X. X. Guo, Y. B. Mo, X. Zhi, F. Y. Kang, Z. Weng and Q. H. Yang, *Adv. Energy Mater.*, 2022, **12**, 8.
4 Z. Su, Z. W. Lu, X. P. Gao, P. W. Shen, X. J. Liu and J. Q. Wang, *J. Power Sources*, 2009, **189**, 411–415.
5 H. L. Pan, Y. Y. Shao, P. F. Yan, Y. W. Cheng, K. S. Han, Z. M. Nie, C. M. Wang, J. H. Yang, X. L. Li, P. Bhattacharya, K. T. Mueller and J. Liu, *Nat. Energy*, 2016, **1**, 7.
6 S. Higashi, S. W. Lee, J. S. Lee, K. Takechi and Y. Cui, *Nat. Commun.*, 2016, **7**, 6.
7 R. Yao, L. Qian, Y. M. Sui, G. Y. Zhao, R. S. Guo, S. Y. Hu, P. Liu, H. J. Zhu, F. C. Wang, C. Y. Zhi and C. Yang, *Adv. Energy Mater.*, 2022, **12**, 10.
8 W. C. Du, E. H. X. Ang, Y. Yang, Y. F. Zhang, M. H. Ye and C. C. Li, *Energy Environ. Sci.*, 2020, **13**, 3330–3360.
9 Y. Chao, C. Liang, H. Q. Tao, Y. R. Du, D. Wu, Z. L. Dong, Q. T. Jin, G. B. Chen, J. Xu, Z. S. Xiao, Q. Chen, C. Wang, J. Chen and Z. Liu, *Sci. Adv.*, 2020, **6**, 13.
10 Z. J. Liu and M. R. Xi, *J. Electrochem. Soc.*, 2022, **169**, 9.
11 D. H. Wang, Q. Li, Y. W. Zhao, H. Hong, H. F. Li, Z. D. Huang, G. J. Liang, Q. Yang and C. Y. Zhi, *Adv. Energy Mater.*, 2022, **12**, 19.
12 Z. X. Liu, Y. Q. Yang, S. Q. Liang, B. A. Lu and J. Zhou, *Small Struct.*, 2021, **2**, 7.
13 Q. Li, B. X. Yan, D. H. Wang, Q. Yang, Z. D. Huang, J. Fan, M. Dai, W. S. Chen and C. Y. Zhi, *Small*, 2022, **18**, 10.
14 Q. Zhang, P. Zhi, J. Zhang, S. Duan, X. Yao, S. Liu, Z. Sun, S. C. Jun, N. Zhao, L. Dai, L. Wang, X. Wu, Z. He and Q. Zhang, *Adv. Mater.*, 2024, **36**, 24.
15 J. Sun, Q. Jian, B. Liu, P. Lin and T. Zhao, *Energy Environ. Mater.*, 2024, e12769.
16 Y. Song, Y. Liu, S. Luo, Y. Yang, F. Chen, M. Wang, L. Guo, S. Chen and Z. Wei, *J. Mater. Chem. A*, 2024, **12**, 6572–6581.
17 M. Gopalakrishnan, S. Ganesan, M. T. Nguyen, T. Yonezawa, S. Praserthdam, R. Pornprasertsuk and S. Kheawhom, *Chem. Eng. J.*, 2023, **457**, 141334.
18 S. R. Motlagh, R. Khezri, A. A. Mohamad, R. Pornprasertsuk, P. Kidkhunthod, M. T. Nguyen, T. Yonezawa and S. Kheawhom, *Mater. Sci. Energy Technol.*, 2023, **6**, 178–191.
19 V. Aupama, W. Kao-ian, J. Sangsawang, G. Mohan, S. Wannapaiboon, A. A. Mohamad, P. Pattananuwat, C. Sriprachuabwong, W.-R. Liu and S. Kheawhom, *Nanoscale*, 2023, **15**, 9003–9013.
20 M. I. Ahmad, D. Bahtiyar, H. W. Khan, M. U. H. Shah, L. Kiran, M. K. Aydinol, M. Yusuf, H. Kamyab and S. Rezania, *J. Energy Storage*, 2023, **72**, 108765.
21 W. J. Hehre, R. Ditchfield and J. A. Pople, *J. Chem. Phys.*, 1972, **56**, 2257–2261.
22 C. Lee, W. Yang and R. G. Parr, *Phys. Rev. B Condens.*, 1988, **37**, 785–789.
23 Z. Y. Liu, X. Wang, T. Lu, A. H. Yuan and X. F. Yan, *Carbon*, 2022, **187**, 78–85.
24 T. Lu and F. Chen, *J. Comput. Chem.*, 2012, **33**, 58–92.
25 T. Lu and S. Manzetti, *Struct. Chem.*, 2014, **25**, 1521–1533.
26 J. Zhang and T. Lu, *Phys. Chem. Chem. Phys.*, 2021, **23**, 20323–20328.
27 T. Lu and F. W. Chen, *J. Mol. Graphics*, 2012, **38**, 314–323.
28 T. Lu and F. Chen, *J. Mol. Graphics Modell.*, 2012, **38**, 314–323.
29 T. Lu and S. Manzetti, *Struct. Chem.*, 2014, **25**, 1521–1533.
30 W. Humphrey, A. Dalke and K. Schulten, *J. Mol. Graphics*, 1996, **14**, 33–38.
31 J. S. Murray and P. Politzer, *Wiley Interdiscip. Rev.: Comput. Mol. Sci.*, 2011, **1**, 153–163.
32 P. Politzer, J. S. Murray and F. A. Bulat, *J. Mol. Model.*, 2010, **16**, 1731–1742.
33 T. Lu and F. Chen, *J. Comput. Chem.*, 2012, **33**, 58–92.
34 X. M. Wang, K. Wang, J. Xu, J. Li, J. E. Lv, M. Zhao and L. M. Wang, *Dyes Pigm.*, 2020, **181**, 12.
35 J. Cao, D. D. Zhang, C. Gu, X. Wang, S. M. Wang, X. Y. Zhang, J. Q. Qin and Z. S. Wu, *Adv. Energy Mater.*, 2021, **11**, 10.
36 B. Beverskog and I. Puigdomenech, *Corros. Sci.*, 1997, **39**, 107–114.
37 K. Wippermann, J. W. Schultze, R. Kessel and J. Penninger, *Cheminform*, 1991, **22**, 205–223.